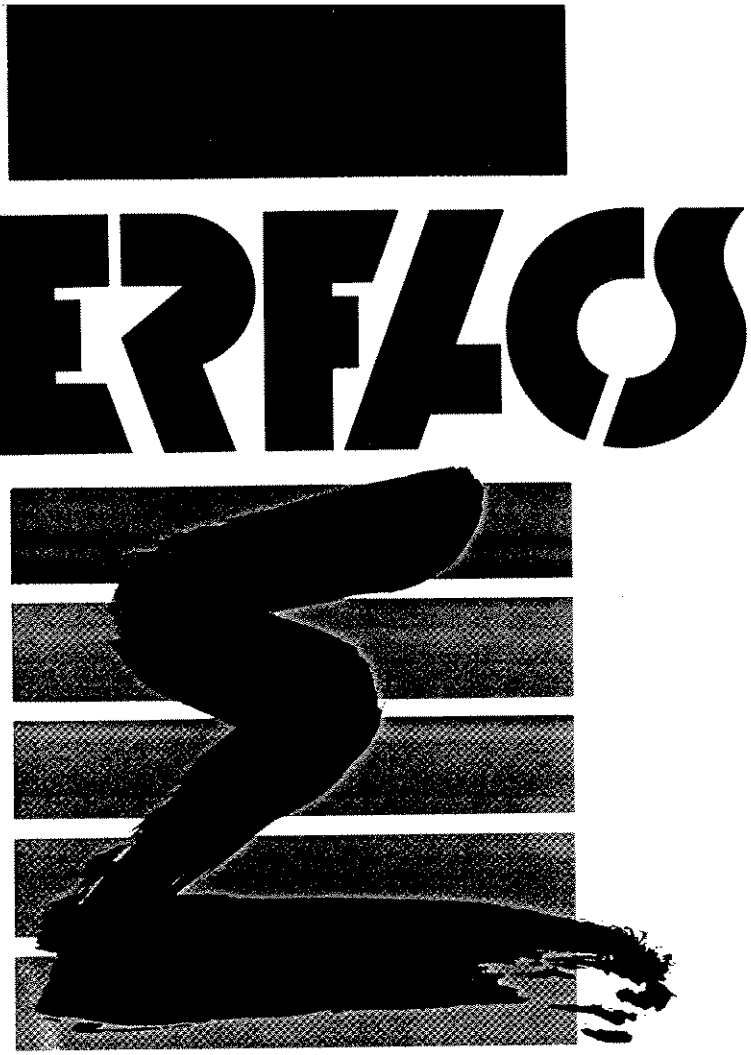

Calculation of the Unsteady Turbulent Flow ehind a Triangular Flameholder

JOHANSSON*, L. DAVIDSON**

Ref : TR/RF/91/53

ermo and Fluid Dynamics, Chalmers University of Technology,
S-412 96 Gothenburg, SWEDEN
** CERFACS, 42 ave Coriolis, 31057 Toulouse, FRANCE

NOMENCLATURE

A	area
a	coefficient in the discretized equations
$c_\mu, c_{1\varepsilon}, c_{2\varepsilon}$	coefficients in the turbulence model
f	frequency (see Eq. 10)
g_{ij}, g^{ij}	the covariant and contravariant components of the metric tensor
H	height of flameholder
$\mathbf{g_i}$	unit base vector tangential to the grid lines (=covariant base vector)
g	determinant of g_{ij}
k	turbulent kinetic energy
$\mathbf{n}$	normal vector
p	pressure
p'	pressure correction
P_k	produktion term in the turbulence model
S^Φ	source term
S_r	Strouhall number (see Eq. 10)
U_i	Cartesian velocity components in the x_i-direction
U, V, W	Cartesian velocity components
U_i'	velocity correction
$\overline{U}, \overline{V}$	mean value of U and V, respectively, during a cycle (see Eq. 11)
$\tilde{U}$	Instantaneous (including turbulent fluctuations) U-velocity
V_i	covariant velocity component
V	volume
x, y, z	Cartesian coordinates

Greek Symbols

δV	volume of control volume
ε	dissipation of turbulent kinetic energy
Φ	general dependent variable
ρ	density
Γ	exchange coefficient
μ	dynamic viscosity
ξ_i	coordinates along (tangential to) the grid lines
ξ, η, ζ	coordinates along (tangential to) the grid lines

Subscripts

$E, P, W, ..$	referring to grid nodes (see Fig. 1)
$e, w, s, ..$	referring to control volume faces (see Fig. 1)
Φ	general dependent variable
t	turbulent
eff	effective

1 INTRODUCTION

The work presented in this report has been carried out at CERFACS in April 1991. Prediction of the flow and combustion in combustion chambers is the aim of an on-going project at Department of Thermo and Fluid Dynamics. The project is carried out in close collaboration with Volvo Flygmotor, Trollhättan, Sweden, where the flow (with and without combustion) behind triangular flameholders has been investigated experimentally using a laser doppler system.

In this work the two-dimensional unsteady flow behind a triangular flameholder is calculated. The combustion is not included. Initially attempts were carried out to solve the steady problem, but no convergent solution was obtained. Furthermore, the experiments showed unsteady flow pattern with vortices being shed from the corners of the flameholder with a well defined Strouhall number. Thus it was decided to solve the unsteady equations. The turbulence is modelled with a $k - \varepsilon$ model.

2 EQUATIONS

The unsteady transport equation in Cartesian coordinates for a general dependent variable reads:

$$\frac{\partial \rho \Phi}{\partial \tau} + \frac{\partial}{\partial x_m}(\rho U_m \Phi) = \frac{\partial}{\partial x_m}(\Gamma_\Phi \frac{\partial \Phi}{\partial x_m}) + \overline{S^\Phi} \qquad (1)$$

where $\overline{S}^{\Phi}$ denotes source per unit volume. If a flux vector J_m containing convection and diffusion is defined as

$$J_m = \rho U_m \Phi - \Gamma_\Phi \frac{\partial \Phi}{\partial x_m} \tag{2}$$

Eq. 1 can be written as:

$$\rho \frac{\partial \Phi}{\partial \tau} + \frac{\partial J_m}{\partial x_m} = \overline{S}^{\Phi}$$

In vector notation the equation reads:

$$\rho \frac{\partial \Phi}{\partial \tau} + \nabla \cdot \mathbf{J} = \overline{S}^{\Phi}$$

Integrating this equation over a volume (with volume V and bounding surface A) using Gauss' law, gives:

$$\int_V \rho \frac{\partial \Phi}{\partial \tau} dV + \int_A \mathbf{J} \cdot \mathbf{dA} = \int_V \overline{S}^{\Phi} dV$$

2.1 Mean Flow Equations

The continuity and unsteady momentum equations in incompressible form reads:

$$\frac{\partial}{\partial x_i}(\rho U_i) = 0$$

$$\frac{\partial}{\partial \tau}(\rho U_i) + \frac{\partial}{\partial x_j}(\rho U_i U_j) = -\frac{\partial p}{\partial x_i} + \frac{\partial}{\partial x_j}(\mu_{eff} \frac{\partial U}{\partial x_j})$$

2.2 The $k - \varepsilon$ Model

The standard high Reynolds $k - \varepsilon$ model is used. The unsteady k and ε-equations have can be written as:

$$\frac{\partial}{\partial \tau}(\rho k) + \frac{\partial}{\partial x_i}(\rho U_i k) = \frac{\partial}{\partial x_i}\{(\mu + \frac{\mu_t}{\sigma_k})\frac{\partial k}{\partial x_i}\} + P_k - \rho\varepsilon$$

$$\frac{\partial}{\partial \tau}(\rho \varepsilon) + \frac{\partial}{\partial x_i}(\rho U_i \varepsilon) = \frac{\partial}{\partial x_i}\{(\mu + \frac{\mu_t}{\sigma_\varepsilon})\frac{\partial \varepsilon}{\partial x_i}\} + \frac{\varepsilon}{k} c_{1\varepsilon}(P_k - c_{2\varepsilon}\rho\varepsilon)$$

The generation term has the form in tensor notation:

$$P_k = \mu_t \frac{\partial U_i}{\partial x_j}(\frac{\partial U_i}{\partial x_j} + \frac{\partial U_j}{\partial x_i})$$

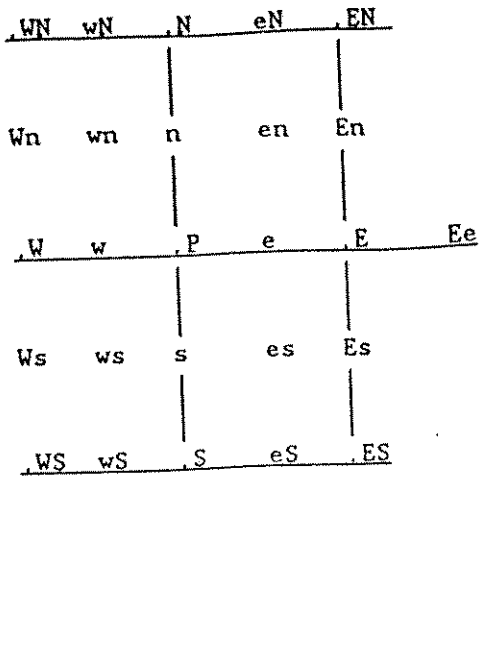

Figure 1: Grid nomenclature. The grid drawn orthogonal for clarity. Dots denote nodes.

The turbulent viscosity is calculated as:

$$\mu_t = \rho c_\mu \frac{k^2}{\varepsilon}$$

and the effective viscosity is obtained as

$$\mu_{eff} = \mu + \mu_t$$

3 THE CODE

In this section the finite volume computer program – **CALC-BFC** (Boundary- Fitted-Coordinates) – for three-dimensional complex geometries is presented. The code is described in [4], and its main features are, for convenience, given below. The program uses Cartesian velocity components, which have been used by e.g. Shyy et al. [16] and Braaten and Shyy [1]. In most finite volume programs staggered grids for the velocity components have been used [11]. In the present work colocated variables are used, which means that all variables are stored at the same location. This concept – suggested by Rhie and Chow [13] – has been used by, for example, Burns and Wilkes [2], Majumdar [8], Majumdar et al. [9], Peric et al. [12], Miller and Schmidt [10], Lien and Leschziner [7].

Equation (2.3) is discretized using standard control volume formulation as described in Patankar [11]. The integration of Eq. (2.3) over a control volume (see Fig. 1) gives

$$(\mathbf{J}\cdot\mathbf{A})_e + (\mathbf{J}\cdot\mathbf{A})_w + (\mathbf{J}\cdot\mathbf{A})_n + (\mathbf{J}\cdot\mathbf{A})_s + (\mathbf{J}\cdot\mathbf{A})_h + +(\mathbf{J}\cdot\mathbf{A})_l = S^\Phi \delta V$$

Note that the positive signs in front of the contributions for the west, south and low faces in Cartesian coordinates are turned into negative ones because the scalar product J · A are then negative.

The discretized equation is obtained as:

$$a_P \Phi_P = \sum a_{nb} \Phi_{nb} + S_C^\Phi \tag{3}$$

where

$$a_P = \sum a_{nb} - S_P^\Phi$$

The coefficents a_{nb} contain contributions due to convection and diffusion, and the source terms S_P^Φ and S_C^Φ contain the remaining terms.

3.1 Time Derivatives

A first order, implicit scheme has been used.

3.2 Convection

The convection, which is the first part of the flux vector **J**, is the scalar product of the velocity vector and the area vector multiplied with the density. For the east face it gives:

$$\dot{m}_e = \rho \mathbf{u} \cdot \mathbf{A} = \rho_e (U_e A_{ex} + V_e A_{ey} + W_e A_{ez})$$

and since the cartesian areas A_{ex}, A_{ey}, A_{ez} are stored the calculation of the convection is straightforward. Special care must, however, be taken when the velocities are interpolated from the nodes to the control volume faces in order to avoid non-physical occilations; Rhie and Chow [13] solved this problem (see also [2], [12] and [10]).

Below is described how the velocities at the control volume faces are calculated. For simplicity, Cartesian coordinates are used.

When the pressure gradient is added to the momentum equation standard linear interpolation is used, i.e.

$$(\frac{\partial p}{\partial x})_P = \frac{p_e - p_w}{\mid \mathbf{we} \mid}$$

where

$$p_e = f_x p_E + (1 - f_x) p_P$$

When calculating the velocity at the east face, for example, the pressure gradient is subtracted so that

$$U_P^\# = U_P - \frac{-(p_e - p_w)\delta V}{\mid \mathbf{we} \mid (a_P)_P}$$

$$U_E^\# = U_E - \frac{-(p_{Ee} - p_e)\delta V}{\mid \mathbf{e(Ee)} \mid (a_P)_E}$$

where a_P is the discretized coefficient in Eq. 3 for the velocities. The U-velocity at the east face is now calculated as:

$$U_e = f_x U_E^\# + (1 - f_x) U_P^\# - \frac{(p_E - p_P)\delta V}{\mid \mathbf{PE} \mid (a_P)_e}$$

The advantage of the last expression of U_e is obvious: now the pressure gradient is calculated using the adjacent nodes of face e. This prevents any non-physical occilations in the pressure field.

The convective terms are discretized using hybrid upwind/central differencing [11].

3.3 Diffusion

Diffusion is the second part of the flux vector $\mathbf{J}$ in Eq. 2, and it has the form:

$$\mathcal{D} = (\mathbf{J} \cdot \mathbf{A})_{diff} = -\Gamma_\Phi \mathbf{A} \cdot \nabla\Phi$$

For the east face, for example, it gives in Cartesian coordinates (x,y,z)

$$-\{\Gamma_\Phi \mathbf{A} \cdot \nabla\Phi\}_e = -\{\Gamma_\Phi (A_x \frac{\partial\Phi}{\partial x} + A_y \frac{\partial\Phi}{\partial y} + A_z \frac{\partial\Phi}{\partial z})\}_e \tag{4}$$

and in curvilinear coordinates (ξ, η, ζ)

$$-\{\mathbf{A} \cdot \nabla\Phi\}_e = -\{\mathbf{A} \cdot \mathbf{g_i} g^{ij} \frac{\partial\Phi}{\partial\xi_j}\}_e = -\{\mid \mathbf{A} \mid \mathbf{n} \cdot \mathbf{g_i} g^{ij} \frac{\partial\Phi}{\partial\xi_j}\}_e \tag{5}$$

The covariant (=tangential) base vectors $\mathbf{g_1}$, $\mathbf{g_2}$ and $\mathbf{g_3}$ correspond to the I, J and K-grid lines, respectively. The metric tensor appears because the components of the product $\mathbf{A} \cdot \mathbf{g_i}$ and the derivative $\partial\Phi/\partial\xi_j$ are both covariant, and the product of their (contravariant) base vectors is not equal to zero or one (as in Cartesian coordinate systems) since they are non-orthogonal to each other [6].

The diffusive terms are discretized using central differencing [11].

3.4 Pressure correction equation

The discretized continuity equation in one-dimension has the form

$$\dot{m}_e - \dot{m}_w = 0 \tag{6}$$

where $\dot{m}$ denotes mass flux, which is calculated as

$$\dot{m} = \rho \mathbf{A} \cdot \mathbf{u}$$

In SIMPLEC [11] the mass flux, $\dot{m}$, is divided into one old value $\dot{m}^*$ and one correction $\dot{m}'$ so that

$$\dot{m} = \dot{m}^* + \dot{m}'$$

The covariant velocity components are in SIMPLEC related to the pressure gradient as [4], [11]

$$V_i = -\frac{1}{a_P} \frac{\partial p}{\partial x_i} \tag{7}$$

The mass flux correction at the east face can now be obtained as:

$$\dot{m}'_e = \rho \mathbf{A} \cdot \mathbf{u}' = \rho_e (A_{ex} u'_e + A_{ey} v'_e + A_{ez} w'_e) = (\rho \mathbf{A} \cdot \mathbf{g}^j V_j)_e$$

Using Eq. 7 gives

$$\dot{m}'_e = \{\rho \mathbf{A} \cdot (-\frac{1}{a_P} \frac{\partial p'}{\partial x_j} \mathbf{g}^j\}_e = -(\frac{\rho}{a_P} \mathbf{A} \cdot \nabla p')_e \tag{8}$$

where p' is the pressure correction. Equations 6 and 8 give

$$(\frac{\rho}{a_P} \mathbf{A} \cdot \nabla p')_w - (\frac{\rho}{a_P} \mathbf{A} \cdot \nabla p')_e + \dot{m}^*_e - \dot{m}^*_w = 0 \tag{9}$$

This equation is a diffusion equation for the pressure correction p'.

4 BOUNDARY CONDITIONS

Inlet:

The velocities have been set according to experiments ($U = 17m/s$, $V = 0$), and k and ϵ have been set from estimations of the turbulence intensity and the turbulent length scale.

Outlet:

The U-velocity is determined from continuity, and the remaining variables are extrapolated.

Walls:

Standard wall functions [14] have been used.

5 RESULTS

The incompressible unsteady two-dimensional flow around and behind a triangular flameholder is calculated. The experiments [15] show that vortices are being shed with a regular and well defined frequence, and a von Kármán street appears behind the flameholder.

In Fig. 2 the grid near the flameholder is shown. The cells in the flameholder are blocked, i.e. all variables are set to zero. One time cycle is approximately $9ms$ (see Fig. 4), and 90 time steps with $\Delta\tau = 0.1ms$ have been used to resolve one cycle.

The calculated pressure contours are shown in Fig. 3 for different times in one cycle. In Fig. 3e approximately one cycle has been compleated and it can be seen that the flow in Fig. 3e is similar to that in Fig. 3a. It is interesting to study the vortices being convected downstream as time increases (from Fig. 3a to 3e). One can, for example, follow the vortex which is located to the right of the upper corner of the flameholder in Fig. 3a (marked with an arrow). As time increases it is convected downstream. At the end of the cycle another vortex is being formed at the same position as in Fig. 3a.

In order to further illustrate the periodicity of the flow field in the calculations the V-velocity below the lower corner of the flameholder is presented as a function of time (see Fig. 4), and

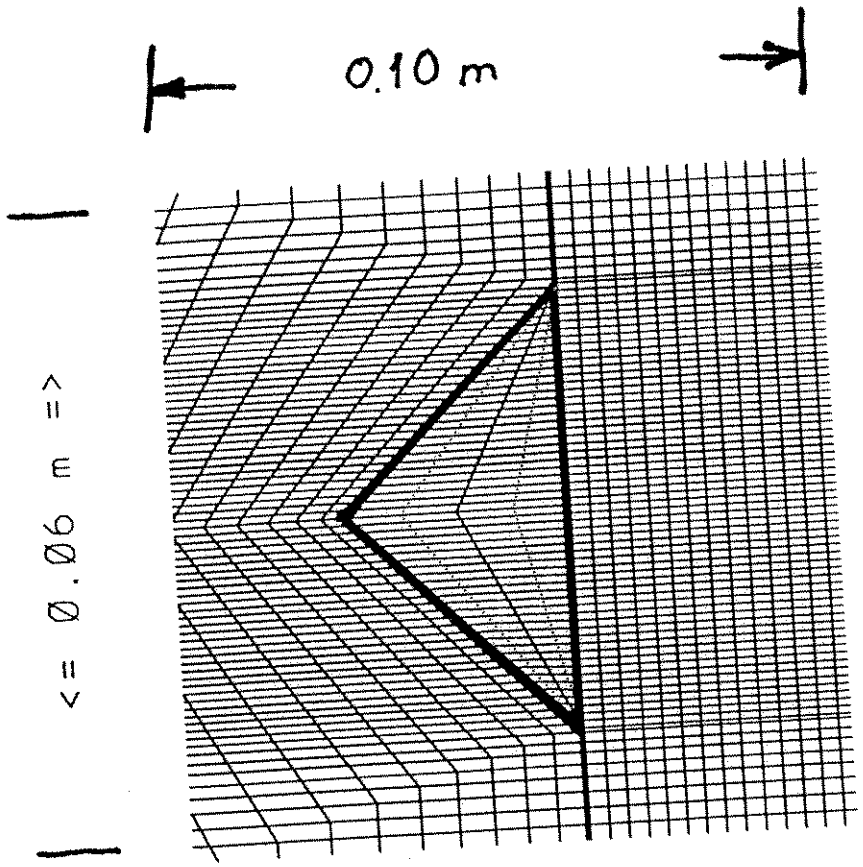

Figure 2: The grid near the flameholder. A 180×100-node grid has been used. Reynolds number based on inlet velocity and height of flameholder is 3.81×10^5. The height of the flameholder is $40mm$; the height of the channel is $120mm$, and its width in the spanwise direction is $240mm$

it can be seen an almost perfect periodicity exists with a constant frequency. The Strouhall number in the calculations

$$S_r = \frac{fH}{U_{in}} \tag{10}$$

is 0.26 which should be compared with experimental one of 0.25 [15]

The predicted velocity vectors are presented in Fig. 5. A large clock-wise vortex with its centre slightly above the centre line can be seen, as well as a small counter clock-wise vortex being formed close to the lower corner of the flameholder.

The calculated U-profiles are compared with the experimental ones in Figs. 6 and 7. As the experimental ones are time averaged, the calculated profiles have been time avergared over one cycle (n time steps). In Fig. 6 the calculated U-velocity at the centre line is compared with the experimental one, and the agreement is good. It is seen that in the predictions the negative maximum is reached slightly too early compared with experiments, and this is also reflected in Fig. 7a where the predicted negative U-velocity near the centre line is too large. Overall, considering the complexity of the problem, the agreement between calculations and experiments is suprisingly good.

In the experiments U_{rms} and V_{rms} have been defined as the sum of cyclic variations in the mean field and the turbulent fluctuations. In order to do any comparisons between calculations and experiments, the predicted total variations in U and V have been calculated, i.e.

$$K_{tot} = < U > + < V > + \frac{1}{n} \Sigma_{l=1}^{n} k_l \tag{11}$$

$$< U > = \frac{1}{n}\Sigma_{\ell=1}^{n}\{\frac{U_\ell - \overline{U}}{2}\}^2$$

$$< V > = \frac{1}{n}\Sigma_{\ell=1}^{n}\{\frac{V_\ell - \overline{V}}{2}\}^2$$

In Fig. 8 the calculated and experimental K_{tot}, together with the cycle averaged calculated turbulent kinetic energy k are shown, and the agreement between calculations and experiments is fairly good. The contribution from the unsteady mean flow to K_{tot} is dominant close to the flameholder. At the first station $x = 15mm$ $< U > + < V >$ is of the same magnitude as k, and further downstream, when the mean flow no longer is constrained by the flameholder, $< U > + < V >$ becomes approximatly twice as big as k. The unsteadiness of the mean flow decays faster than the turbulent kinetic energy and at $376mm$ behind the flameholder k is larger than $< U > + < V >$.

6 CONCLUSIONS

The two-dimensional, unsteady, incompressibel flow has been numerically simulated. A computer code based on pressure-correction procedure, written in non-orthogonal coordinates, solving for the Cartesian coordinates, has been used. An important feature of the code is that – contrary to many SIMPLE codes – it is using non-staggered grids for the velocity components. For space discretization hybrid central/upwind differencing has been used for the convective terms, and central differencing for the diffusion terms. First order fully implicit has been used for time discretization. The turbulence has been modelled using a standard high Reynolds number $k - \varepsilon$ model. Wall functions have been used at all walls.

The calculated results have been compared with experimental data, obtained with laser-doppler system. The experiments show that the mean flow behind the flameholder is unsteady, and that a von Kármán street is formed with a well defined Strouhall freqency.

The following conclusions can be drawn:

- the predicted results show – as found in the experiments – a von Kármán street behind the flameholder
- the experimentally observed Strouhall number (=0.25) is very well captured in the predictions (=0.26)
- the calculated velocity profiles agree well with the experiments
- the calculated velocities variations in time agree also well with the experiments
- it was found that a rather fine mesh (180) was needed to resolve the velocity scales

ACKNOWLEDGEMENTS

This project is sponsored by The Swedish Board for Technical Development (STU) and The National Energy Administration (STEV). STU has, in the context of the STU-CERFACS collaboration, financed the travel expensis for Stefan Johansson.

7 REFERENCES

References

[1] **M. BRAATEN and W. SHYY**, A study of recirculating flow computation using body-fitted coordinates: consistency aspects and mesh skewness, *Numer. Heat Transfer*, 9, 559-574, 1986.

[2] **A.D. BURNS and N.S. WILKES**, A finite difference method for the computation of fluid flows in complex three dimensional geometries, AERE R 12342, Harwell Laboratary, England, 1987.

[3] **L. DAVIDSON**, CALC-BFC: A finite-volume code for complex three- dimensional geometries using colocated variables and cartesian velocity components, Rept., Dept. of Applied Thermodynamics and Fluid Mechanics, Chalmers University of Technology, Gothenburg, 1989.

[4] **L. DAVIDSON and P. Hedberg**, Mathematical derivation of a finite-volume formulaton for laminar flow in complex geometries, *Int. J. Numer. Methods Fluids*, 9, 531-540, 1989.

[5] **W. FLÜGGE**, Tensor analysis and continuum mechanics, Springer-Verlag, Berlin, 1972.

[6] **F. IRGENS**, Tensoranalyse og kontinuumsmekanikk, (in Norwegian), del III, Institutt for mekanikk, Norges Tekniska Høgskole, Trondheim, 1966.

[7] **F.S. LIEN and M.A. LESCHZINER**, Multigrid convergence acceleration for complex flow including turbulence, Third European Conf. on Multigrid Methods, Bonn, October 1990.

[8] **S. MAJUMDAR**, Development of a finite volume procedure for prediction of fluid flow problems with complex irregular boundaries, SFB 210/T/29, Sonderforschungsbereich 210, University of Karlsruhe, 1986.

[9] **S. MAJUMDAR, W. RODI, and S.P. VANKA**, On the use of non-staggered pressure-velocity arrangement for numerical solution of incompressible flows, SFB 210/T/35, Sonderforschungsbereich 210, University of Karlsruhe, 1987.

[10] **T.F. MILLER and F.W. SCHIMDT**, Use of a pressure-weighted interpolation method for the solution of the incompressible Navier-Stokes equations on a nonstaggered grid system, *Numer. Heat Transfer*, 14, 213-233, 1988.

[11] **S.V. PATANKAR**, Numerical heat transfer and fluid flow, McGraw-Hill, Washington, 1980.

[12] **M. PERIC, R. KESSLER, and G. SCHEURER**, Comparison of finite-volume numerical methods with staggered and colocated grids, *Computers & Fluids*, **16**, 389-403, 1988.

[13] **C.M. RHIE and W.L. CHOW**, Numerical study of the turbulent flow past an airfoil with trailing edge separation, *AIAA J.*, **21**, 1527-1532, 1984.

[14] **W. Rodi**, Turbulence models and their application in hydraulics, International Association of Hydraulic Research, Monograph, Delft (1980).

[15] **A. SJUNNESSON**, private communication, Volvo Flygmotor, Trollhättan, Sweden.

[16] **W. SHYY, S.S. TONG, and S.M. CORREA**, Numerical recirculating flow calculation using body-fitted coordinate system, *Numer. Heat Transfer*, 8, 99-113, 1985.

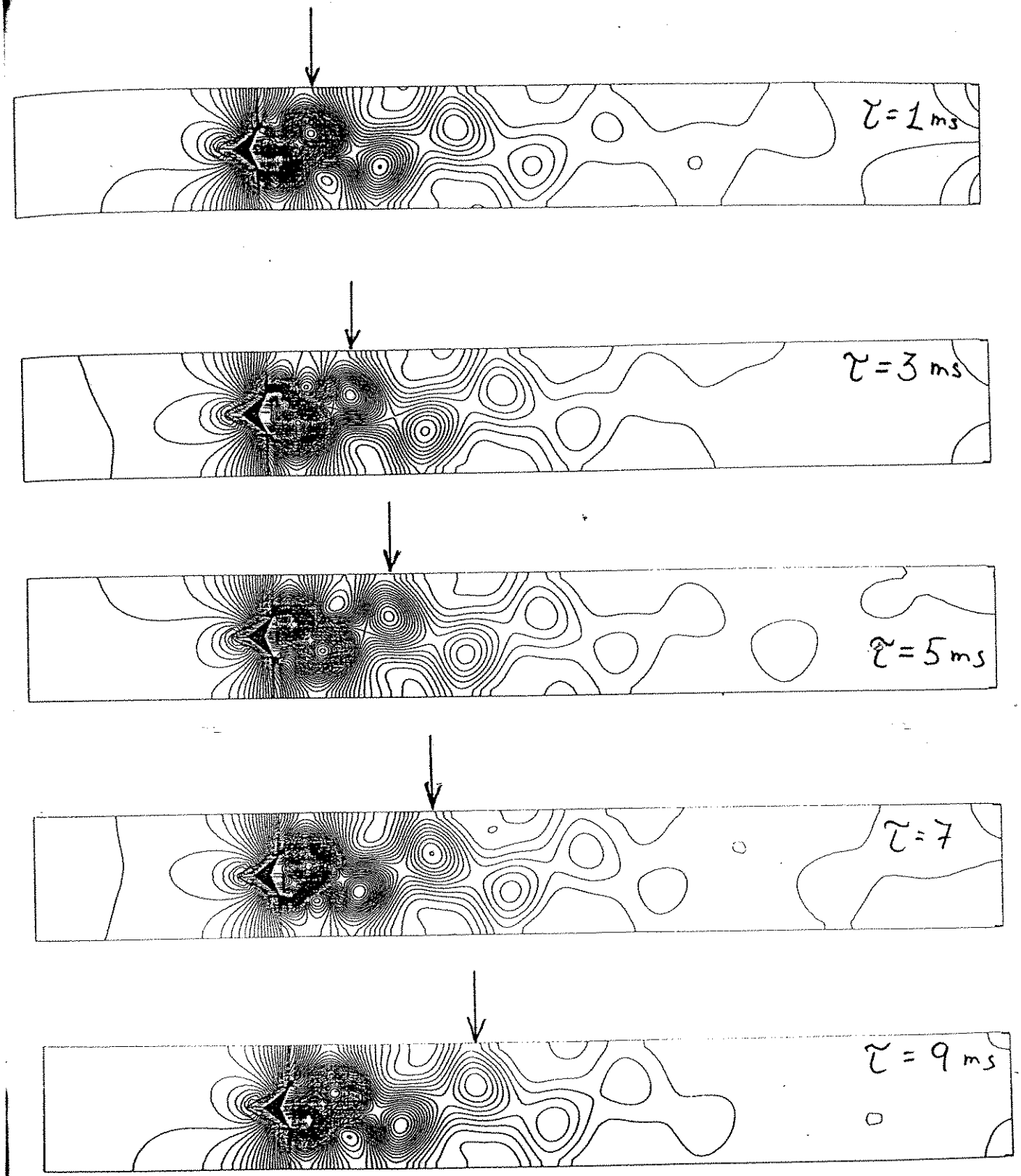

Figure 3: Predicted pressure contours at different times. An arrow above each figure indicates at each time the position of a chosen vortex. a) $\tau = 1ms$, b) $\tau = 3ms$, c) $\tau = 5ms$, d) $\tau = 7ms$, e) $\tau = 9ms$. The cycle time is approximately $9ms$

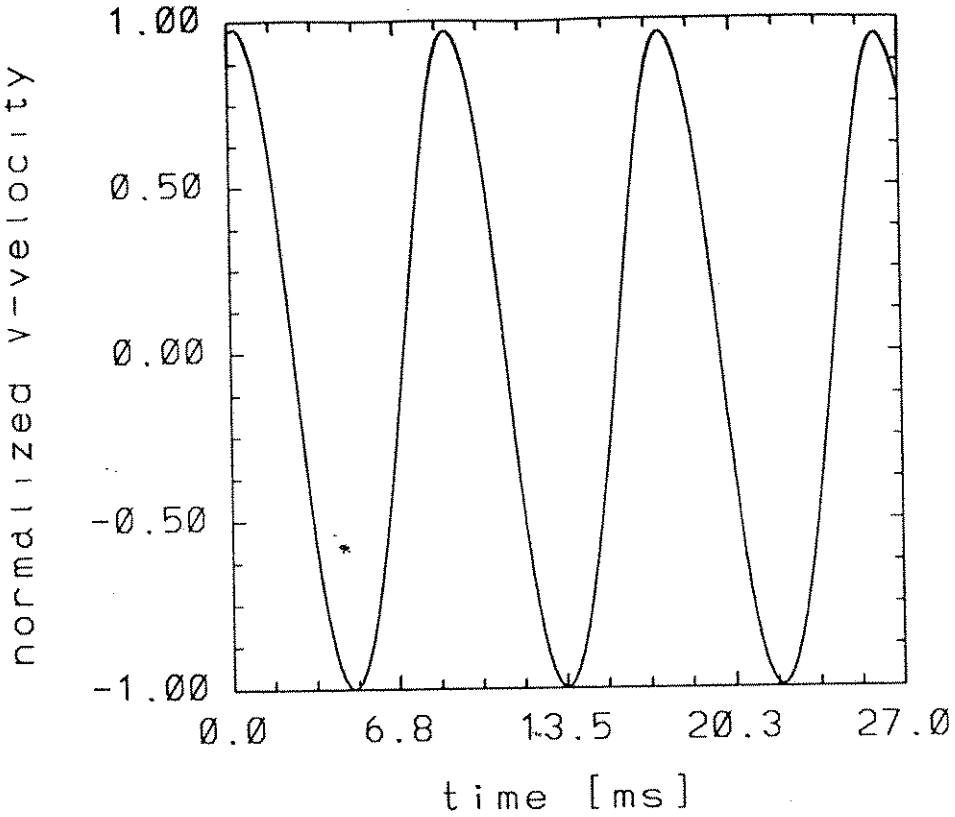

Figure 4: Predicted normalized V-velocity at one point (9 mm behind and 40 mm below the lower corner of the flameholder) as function of time.

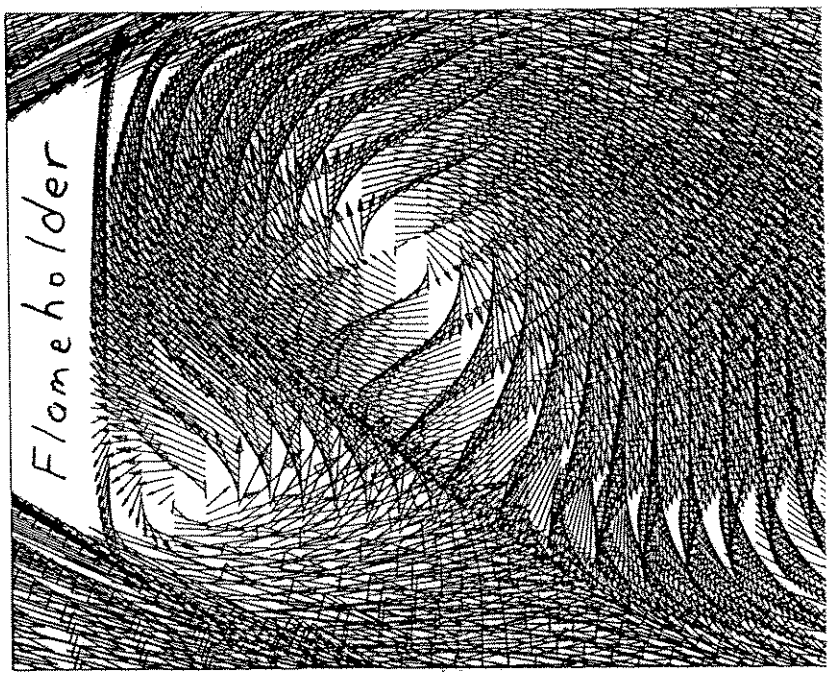

Figure 5: Predicted velocity vectors behind the flameholder

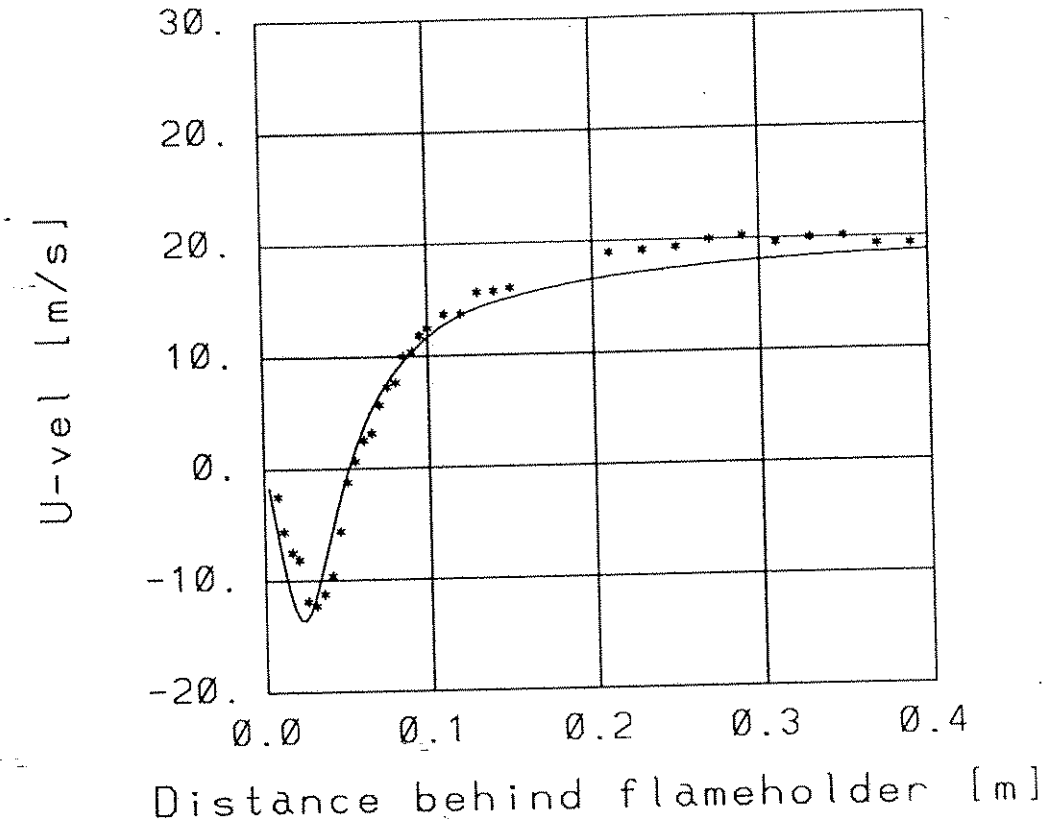

Figure 6: Time averaged U-velocity at the centre line behind the flameholder. ——, calculations. $*$, experiments.

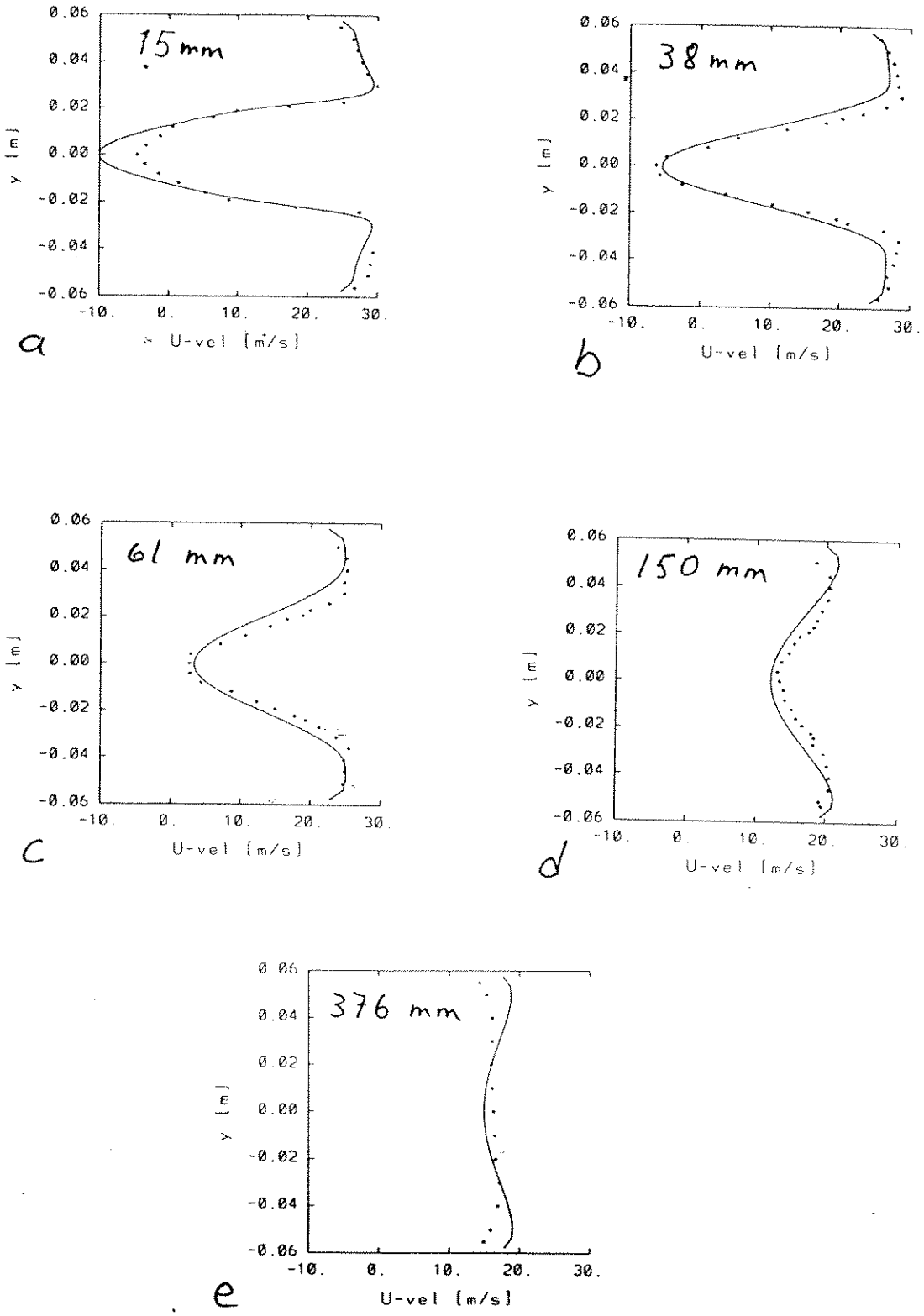

Figure 7: Time averaged U-velocity. ——, calculations. $*$, experiments. a) 15 mm behind flameholder, b) 38 mm, c) 61 mm, d) 150 mm, e) 376 mm.

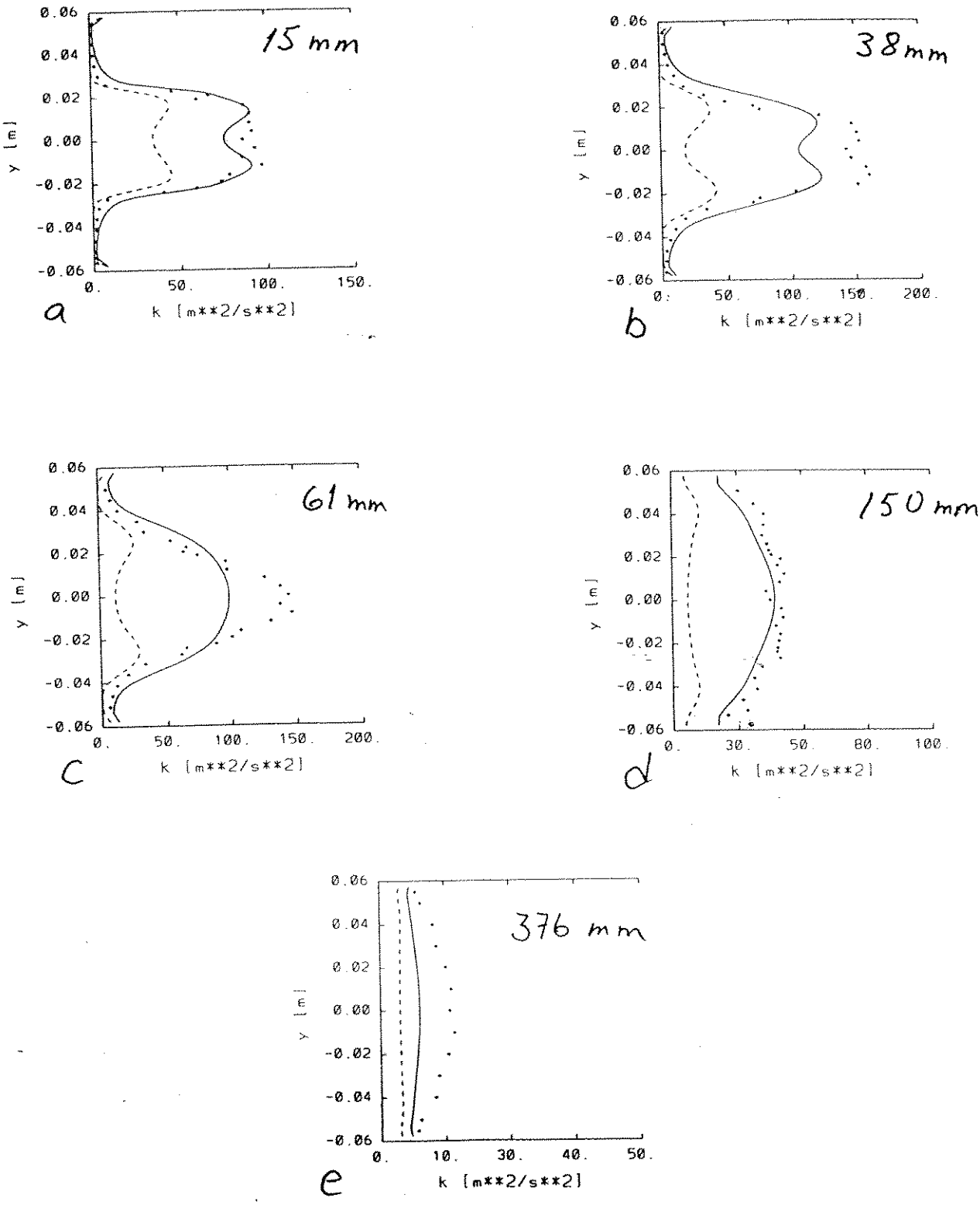

Figure 8: Predicted and experimental K_{tot} together with predicted cycle averaged k. ——, predicted K_{tot} (see Eq. 11), – – ––, predicted k, $*$, experimental K_{tot}. a) 15 mm behind flameholder, b) 38 mm, c) 61 mm, d) 150 mm, e) 376 mm.